

Reactive fibrosis precedes doxorubicin-induced heart failure through sterile inflammation

Ryo Tanaka^{1,2}, Masanari Umemura^{1,2*}, Masatoshi Narikawa^{1,2}, Mayu Hikichi¹, Kohei Osaw¹, Takayuki Fujita^{1,2}, Utako Yokoyama³, Tomoaki Ishigami², Kouichi Tamura² and Yoshihiro Ishikawa^{1*}

¹Cardiovascular Research Institute, Yokohama City University School of Medicine, Yokohama, Japan; ²Medical Science and Cardiorenal Medicine, Yokohama City University School of Medicine, Yokohama, Japan; ³Department of Physiology, Tokyo Medical University, Tokyo, Japan

Abstract

Aims Doxorubicin (DOX)-induced heart failure has a poor prognosis, and effective treatments have not been established. Because DOX shows cumulative cardiotoxicity, we hypothesized that minimal cardiac remodelling occurred at the initial stage in activating cardiac fibroblasts. Our aim was to investigate the initial pathophysiology of DOX-exposed cardiac fibroblasts and propose prophylaxis.

Methods and results An animal study was performed using a lower dose of DOX (4 mg/kg/week for 3 weeks, i.p.) than a toxic cumulative dose. Histological analysis was performed with terminal deoxynucleotidyl transferase-mediated dUTP nick-end labelling assay, picosirius red staining, and immunohistochemical staining. The mechanism was analysed *in vitro* with a low dose of DOX, which did not induce cell apoptosis. Microarray analysis was performed. Differentially expressed genes were confirmed by enrichment analysis. Mitochondrial damage was assessed by mitochondrial membrane potential. The production of inflammatory cytokines and fibrosis markers was assessed by western blot, quantitative polymerase chain reaction, and ELISA. A phosphokinase antibody array was performed to detect related signalling pathways. Low-dose DOX did not induce cell death, and fibrosis was localized to the perivascular area in mice. Microarray analysis suggested that DOX induced genes associated with the innate immune system and inflammatory reactions, resulting in cardiac remodelling. DOX induced mitochondrial damage and increased the expression of interleukin-1. DOX also promoted the expression of fibrotic markers, such as alpha smooth muscle actin and galectin-3. These responses were induced through stress-activated protein kinase/c-Jun NH2-terminal kinase signalling. A peroxisome proliferator-activated receptor (PPAR γ) agonist attenuated the expression of fibrotic markers through suppressing stress-activated protein kinase/c-Jun NH2-terminal kinase. Furthermore, this molecule also suppressed DOX-induced early fibrotic responses *in vivo*.

Conclusions Low-dose DOX provoked reactive fibrosis through sterile inflammation evoked by the damaged mitochondria.

Keywords Anticancer drugs; Cardiac fibroblast; Remodelling; Inflammation; Pathophysiology

Received: 7 August 2019; Revised: 6 December 2019; Accepted: 22 December 2019

*Correspondence to: Masanari Umemura and Yoshihiro Ishikawa, Cardiovascular Research Institute, Yokohama City University School of Medicine, Yokohama, Japan.

Email: umemurma@yokohama-cu.ac.jp; yishikaw@med.yokohama-cu.ac.jp

Introduction

At present, medical advancements have improved the prognosis of cancer-bearing patients. As the number of cancer survivors increases, cardiovascular events associated with anticancer drugs are also increasing; therefore, this issue is recognized as a serious problem.^{1,2} Anthracycline antibiotics are known to provoke heart failure.³ Doxorubicin (DOX), a representative anthracycline antibiotic, is an efficacious and

widely used chemotherapeutic agent. However, the prophylaxis and its treatments for cardiotoxicity are still unknown. Some studies have reported the molecular mechanisms of DOX cardiomyopathy. They demonstrated DOX-induced DNA damage, accumulation of reactive oxygen species, iron accumulation in mitochondria,⁴ abnormality of intracellular calcium dynamics,⁵ inhibition of topoisomerase 2 β , and so forth.⁶ However, the major pathogenesis has not yet been completely elucidated. The terminal stage of DOX-induced

cardiotoxicity pathologically resembles the features of dilated cardiomyopathy, for example, vacuole degeneration of myocytes, shedding of myofibrils, and fibrosis. However, the initial change and the pathological progression are still unknown.

Cardiac fibroblasts (CFs) account for 60–70% of the heart and play a central role in extracellular matrix (ECM) remodeling.⁷ CFs induce ‘replacement fibrosis’ in the cell shedding part, such as in myocardial infarction.⁸ Dead cells are replaced, and scars are formed that mainly contain collagen type I. Then, the tissue defect region is mechanically stabilized. In contrast, CFs, which are continuously activated by chronic load and inflammation, such as hypertension and diabetes, induce ‘reactive fibrosis’.⁹ Reactive fibrosis leads to an increased ECM deposition without a significant loss of cells. Initially, reactive fibrosis occurs in perivascular area that later spreads to interstitial zone. DOX-induced heart failure often develops in the remote phase.¹⁰ DOX-induced cardiotoxicity is also cumulative.¹¹ Therefore, we expect that the continuous activation of CFs by this inflammation contributes to the development of cardiotoxicity and ‘reactive fibrosis’ at the low-dose accumulation stage. However, there are few reports focusing on ‘reactive fibrosis’ instead of ‘replacement fibrosis’.

Here, we sought to determine the direct effects of DOX at the initial stage before reaching the toxic dose on CFs, that is, not ‘replacement fibrosis’ but ‘reactive fibrosis’. In addition, we proposed prophylaxis focusing on CFs.

Methods

Reagents

Galectin-3 antibody, SAPK/JNK antibody, phospho-SAPK/JNK (Thr183/Tyr185) antibody, Phospho-PI3 Kinase Class III (Ser249) antibody, PI3 Kinase Class III antibody, SQSTM1/p62 antibody, LC3B antibody, and glyceraldehyde-3-phosphate dehydrogenase (GAPDH) antibody were purchased from Cell Signaling (Danvers, MA, USA). Collagen type 1A1 (COL1A1) antibody and interleukin (IL)-1R-associated kinase 1 (IRAK-1) were purchased from Santa Cruz (Dallas, TX, USA). The α -SMA antibody was purchased from Sigma-Aldrich (St. Louis, MO, USA). Alexa Fluor 488 goat anti-mouse immunoglobulin G (IgG) and Alexa Fluor 594 goat anti-rabbit immunoglobulin G were purchased from Invitrogen (Carlsbad, CA, USA). DOX hydrochloride and SP600125 were purchased from Sigma-Aldrich. Chloroquine was purchased from Thermo Fisher Scientific (Waltham, MA, USA). Pioglitazone hydrochloride was purchased from Fujifilm (Tokyo, Japan). ODN2088 and GW1929 were purchased from AdipoGen Life Sciences (San Diego, CA, USA).

Animal study

Seven-week-old male C57BL/6J mice were purchased from Japan SLC (Shizuoka, Japan). Mice were randomly allocated into two or three groups (each group consisted of four mice) as follows: normal saline group (NS), DOX-treated group (DOX), or DOX and pioglitazone-treated group (DOX + Pio). DOX was administered intraperitoneally (4 mg/kg/week for 3 weeks, i.p.), and pioglitazone was administered orally (10 mg/kg/day for 4 weeks, p.o.). After 4 weeks of DOX administration, all mice were euthanized under isoflurane anaesthesia (2%), and the heart was rapidly excised. The left ventricle was fixed in 10% formaldehyde solution.

Histological analysis

Left ventricle tissues were fixed with formalin, embedded in paraffin, and sectioned at 3.5 μ m thickness. Cell apoptosis in the cardiac tissue was evaluated using the terminal deoxynucleotidyl transferase-mediated dUTP nick-end labeling (TUNEL) assay. TUNEL Apoptosis Assay Kit was performed using the DeadEnd Fluorometric TUNEL System (Madison, WI, USA). All nuclei were visualized with DAPI. Cells were then visualized using fluorescence microscopy with an inverted microscope (Nikon, Tokyo, Japan). The TUNEL-positive area as cell apoptosis in cardiac tissue was measured by ImageJ software (NIH, MD, USA). Three random fields were calculated. Collagen deposition was evaluated with the Picrosirius Red Stain Kit (ScyTek Laboratories, UT, USA). The expression of α -SMA was evaluated by immunohistochemical staining. The perivascular fibrotic area in three random fields was measured by ImageJ software. The expression of α -SMA and galectin-3 in the perivascular area was evaluated by immunohistochemical staining. Three random fields were quantitatively evaluated by ImageJ software.

Ethics statement

Animal studies were performed according to the Yokohama City University guidelines. The Animal Care and Use Committee at Yokohama City University School of Medicine approved all animal studies and experimental protocols.

Cell culture

Human CFs (HCFs) were purchased from ScienCell Research Laboratories (Carlsbad, CA, USA). HCFs were cultured in fibroblast medium-2 (ScienCell Research Laboratories), a commercial fibroblast medium supplemented with 1% penicillin/streptomycin, 1% fibroblast growth supplement-2, and 2% foetal bovine serum.¹² All cells were maintained in

a humidified atmosphere of 95% air and 5% CO₂ at 37 °C. The 4th through 8th passages of HCFs were used for the experiments.

Cell proliferation assay

The XTT Cell Proliferation Kit (ATCC, VA, USA) was used to analyse cell proliferation, as previously reported.¹³

Cell viability and apoptosis assay

The Calcein-AM Kit and Propidium Iodide Kit (Sigma-Aldrich, MO, USA) were used to analyse cell viability and apoptosis, as previously reported.¹⁴ Staining intensity area (green) and staining cell numbers (red) in four random fields were measured by ImageJ software (MD, USA).

Microarray

Human CFs were exposed to 0.1 μM DOX for 6 h or 24 h, and total RNA was extracted. Microarray experiments were carried out using a SurePrint G3 Human GE 8x60K v3 Microarray and a SurePrint G3 Mouse Gene Expression 8x60K v2 Microarray (Agilent Technologies, CA, USA) according to the manufacturer's protocol.

Bioinformatics analysis

Genes that were increased more than 1.5-fold by DOX treatment were analysed using the Database for Annotation, Visualization and Integrated Discovery (version 6.8, <https://david.ncifcrf.gov>). Genes were analysed with the Kyoto Encyclopedia of Genes and Genomes (KEGG) and Gene Ontology pathway databases. To investigate the activated genes of biological functions in DOX-exposed HCFs, gene set enrichment analysis (GSEA, <http://software.broadinstitute.org/gsea/index.jsp>) was performed. The gene sets used for analysis were the Molecular Signatures Database (MSigDB) of c5 (c5.all.v6.2.symbol.gmt).

Mitochondrial membrane potential assay

MitoTracker Red CMXRos (Invitrogen, Carlsbad, CA, USA) was used to analyse mitochondrial membrane potential. HCFs were preincubated with 100 nM of MitoTracker Red. Cells were then visualized using fluorescence microscopy with an inverted microscope (Nikon, Tokyo, Japan). Staining intensity was quantified using ImageJ software (NIH). MitoTracker Red staining intensity of multiple fields was quantified with ImageJ (NIH) and measured using a microplate reader

equipped with a spectrofluorometer (PerkinElmer, Waltham, MA, USA) at an emission wavelength of 615 nm and excitation wavelength of 550 nm.

Mitophagy assay

Human CFs were incubated with 100 nM Mitophagy Dye working solution. Then, HCFs were incubated with or without DOX for 6 and 24 h. HCFs were incubated with 1 μM Lyso Dye working solution. Cells were then visualized using fluorescence microscopy with an inverted microscope. This assay was performed using the Mitophagy Detection Kit (Dojindo, Kumamoto, Japan). Staining intensity was quantified using ImageJ software (NIH). Mitophagy Dye staining intensity of multiple fields was quantified with ImageJ (NIH). Colocalization analysis of Mitophagy Dye and Lyso Dye was evaluated by Spearman's rank correlation coefficient with Image-J.

Quantitative real-time reverse transcription polymerase chain reaction

Total RNA from HCFs was extracted using the RNAiso Plus reagent (TaKaRa Bio, Shiga, Japan), and reverse transcription reactions were performed using the PrimeScript RT reagent kit (TaKaRa Bio), as previously described.¹⁵ Quantitative polymerase chain reaction (qPCR) was prepared using SYBR Fast qPCR Mix (TaKaRa Bio). Reverse transcription–polymerase chain reaction was performed on the StepOnePlus Real-Time PCR System (Applied Biosystems, CA, USA). The 2^{-ΔΔCt} method was used to determine relative gene expression levels using 18S to normalize the data. The sequences of the specific primers are shown in Supporting Information, *Table S1*.¹²

Mitochondrial DNA copy number

Mitochondrial copy numbers were quantified in genomic DNA using SYBR green-based qPCR. DNA was isolated using the genomic DNA extraction kit (Qiagen, VA, USA), and mtDNA copy number was quantified with the aforementioned quantitative PCR and the comparative Ct method using nuclear DNA content as a standard. The sequences of specific primers to the mtDNA (GenBank accession no. MK033602) and nuclear DNA (GenBank accession no. NM004048) are shown in *Figure 4J*.

Western blotting

Western blotting was performed as previously described.¹⁵ GAPDH antibody was used as loading controls to normalize

Figure 1 Low-dose DOX induced reactive fibrosis in mice. (A) Protocol in experiments to assess the DOX-induced cardiotoxicity in mice. The total cumulative dose of DOX was set to 12 mg/kg. Saline (control) or DOX (4 mg/kg/week for 3 weeks) was administered intraperitoneally. (B, D) TUNEL apoptosis assay of heart sections; The apoptotic area was quantitatively assessed in three random fields (unpaired *t*-test, *n* = 4, *n.s.: no significant difference). (C, E) Sirius red staining of heart sections; magnification = ×40. Perivascular fibrosis was assessed quantitatively in three random fields (unpaired *t*-test, *n* = 4, **P* < 0.05).

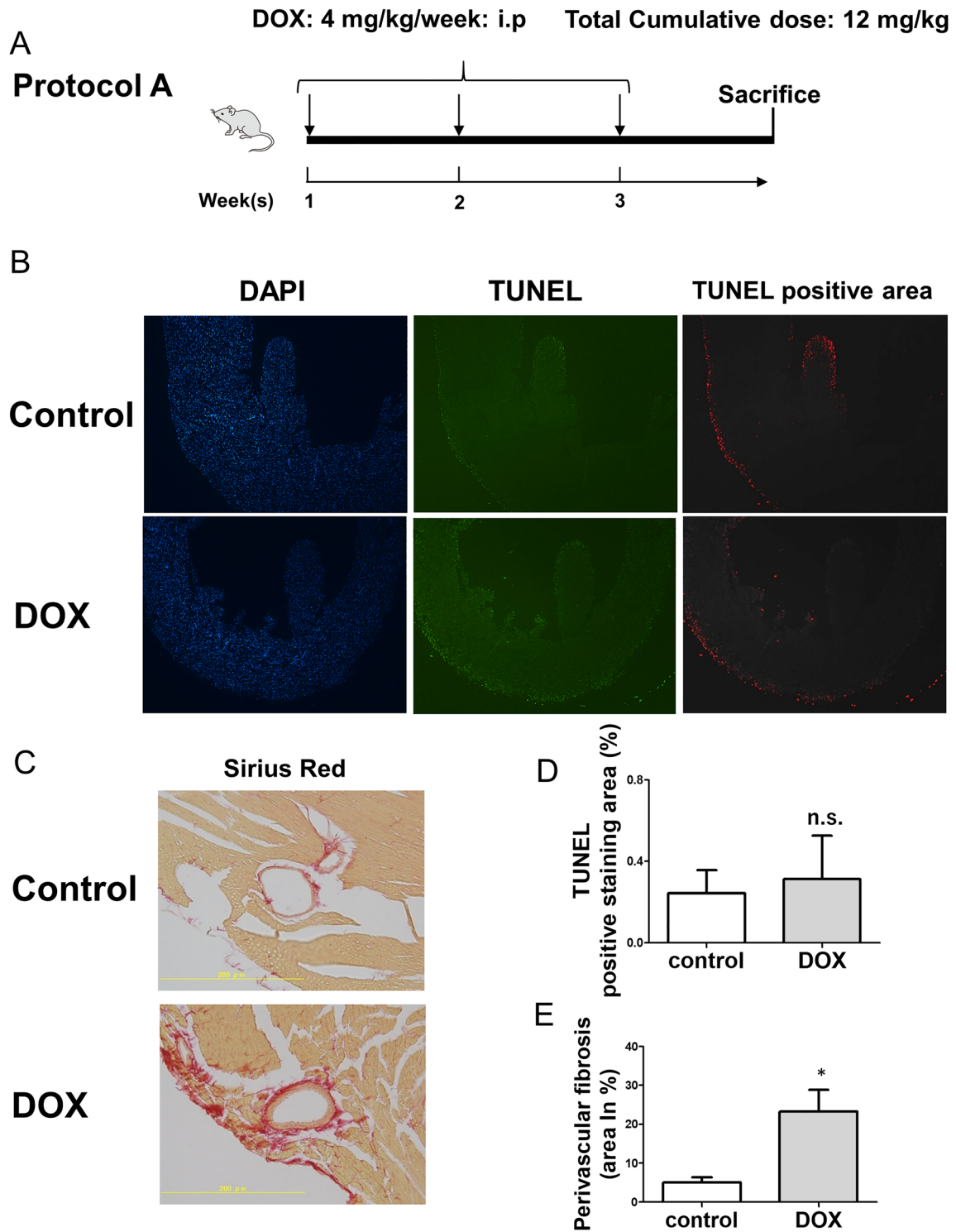


Figure 2 Enrichment analysis and gene expression induced by low-dose DOX in HCFs. (A–C) HCFs were exposed to DOX (0.1 μ M) for 24 h, and cell viability and apoptosis were evaluated with Calcein-AM and propidium iodide assays. Staining intensity area (green) and stained cell numbers (red) in four random fields were measured by ImageJ software (one-way ANOVA with Tukey’s *post hoc* test, $n = 4$, *** $P < 0.001$, n.s.: no significant difference). (D) HCFs were exposed to DOX (0.1 to 1.0 μ M) for 24 h, and cell proliferation was measured with an XTT assay (one-way ANOVA with Tukey’s *post hoc* test, $n = 4$, *** $P < 0.001$, n.s.: no significant difference). HCFs were exposed to 0.1 μ M DOX for 6 and 24 h, and mRNA expression levels were analysed with a microarray. (E) Number of differentially expressed transcripts that changed >1.5 -fold and <0.67 -fold at 6 and 24 h. (F) The table shows the top 10 KEGG pathways that were significantly enriched in upregulated genes at 24 h. Red letters are terms related to the inflammatory and innate immune system. (G) GSEA suggested that gene sets associated with the inflammatory and innate immune system were upregulated at 24 h. The gene sets were ‘POSITIVE_REGULATION_OF_INFLAMMATORY_RESPONSE’, ‘CYTOKINE_ACTIVITY’, ‘RESPONSE_TO_BACTERIUM’, ‘POSITIVE_REGULATION_OF_RESPONSE_TO_WOUNDING’, and ‘LYTIC_VACUOLE’. (H) Inflammatory cytokine-associated gene and TLR family expression in HCFs at 6 and 24 h. (I) Cardiac remodelling-associated gene expression in HCFs at 6 and 24 h.

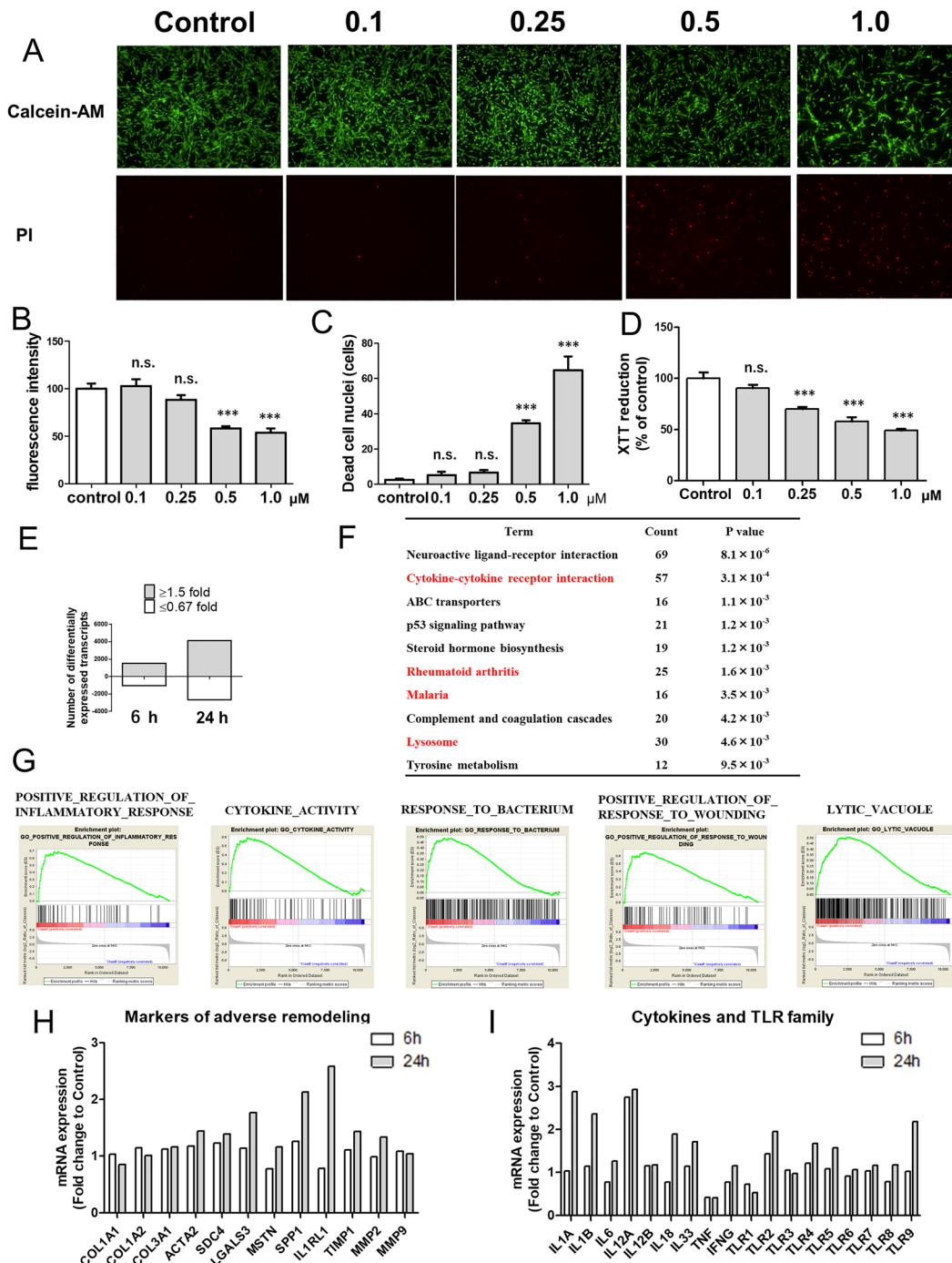


Figure 3 DOX decreased the mitochondrial membrane potential and induced mitophagy and compensatory reactions in the early phase. (A) Evaluation of mitochondrial activity in DOX-exposed HCFs. Red fluorescence is MitoTracker Red, depending on the mitochondrial membrane potential of living cells. (B) MitoTracker Red staining intensity of multiple fields was quantified with ImageJ (unpaired *t*-test, *n* = 9, ****P* < 0.001). (C) MitoTracker Red staining intensity of multiple fields was measured using a microplate reader equipped with a spectrofluorometer at an emission wavelength of 615 nm and excitation wavelength of 550 nm (unpaired *t*-test, *n* = 8, **P* < 0.05). (D) Evaluation of mitophagy in DOX-exposed HCFs. Red fluorescence is a mitophagy staining dye (Mitophagy Dye), which emits high fluorescence when mitophagy is induced and the damaged mitochondria fuse to lysosomes. Green fluorescence is lysosomal staining dye (Lyso Dye), which shows colocalization between the Mitophagy Dye-labelled mitochondria and the lysosome. (E) Mitophagy Dye staining intensity of multiple fields was quantified with ImageJ (unpaired *t*-test, *n* = 16, ****P* < 0.001). (F) Colocalization analysis of Mitophagy Dye and Lyso Dye was evaluated by Spearman's rank correlation coefficient with ImageJ (*n* = 16, ****P* < 0.001). (G) TFAM mRNA expression in HCFs with or without DOX treatment (0.1 μM) for 6, 12, and 24 h (unpaired *t*-test, *n* = 4–7, **P* < 0.05, ***P* < 0.01, ****P* < 0.001). (H) Mitochondrial DNA copy number in HCFs with or without DOX treatment (0.1 μM) for 6, 12, and 24 h (unpaired *t*-test, *n* = 4–11, **P* < 0.05, ***P* < 0.01, ****P* < 0.001, n.s.: no significant difference). (I–L) Protein expression of Phospho-PI3 Kinase Class III (p-PI3KC3), p62, and LC3 in HCFs stimulated by DOX (0.1 μM) for 24 h (unpaired *t*-test, *n* = 4, **P* < 0.05, ****P* < 0.001).

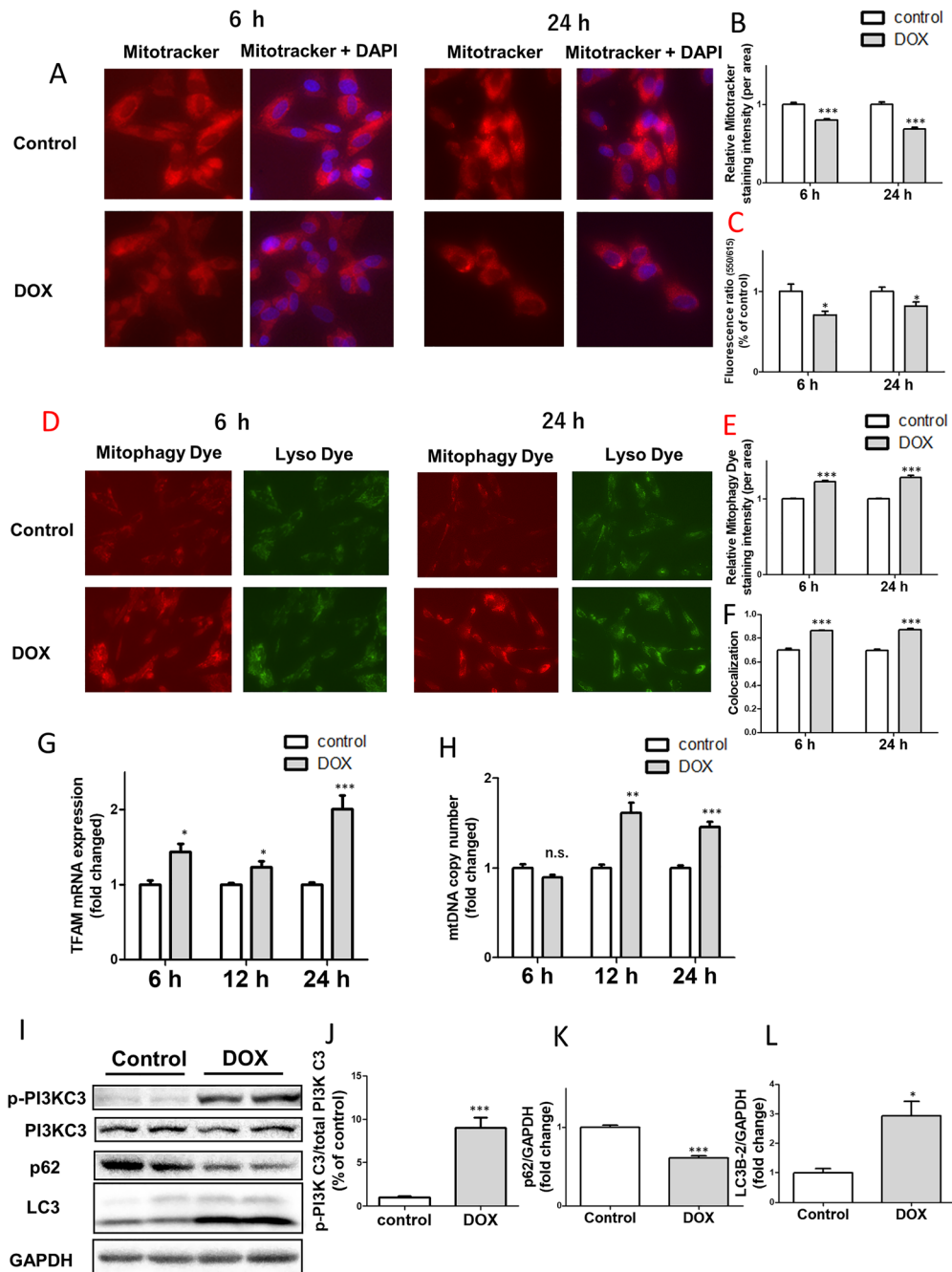


Figure 4 DOX increased the mRNA expression of TLR9, IL-1, and fibrotic markers, and chloroquine attenuated its response in HCFs. (A–E) TLR9, IL-1 β , ACTA2, LGAL3, and TIMP-1 mRNA expression in HCFs with or without DOX treatment (0.1 μ M) for 6, 12, and 24 h (unpaired *t*-test, $n = 4$ –17, * $P < 0.05$, ** $P < 0.01$, *** $P < 0.001$, n.s.: no significant difference). (F–I) IL1B, ACTA2, LGAL3, and TIMP-1 mRNA expression in HCFs exposed to DOX (0.1 μ M) with or without ODN2088 (1 μ M) for 6, 12, and 24 h (one-way ANOVA with Tukey's *post hoc* test, $n = 4$, *** $P < 0.001$). (J–M) IL1B, ACTA2, LGAL3, and TIMP-1 mRNA expression in HCFs exposed to DOX (0.1 μ M) in the absence or presence of chloroquine (10 μ M) for 6, 12, and 24 h (one-way ANOVA with Tukey's *post hoc* test, $n = 5$, * $P < 0.05$, *** $P < 0.001$). (N) The secretion of IL-1 β in HCFs exposed to DOX (0.1 μ M) with or without ODN2088 (1 μ M) or chloroquine (10 μ M) for 24 h (one-way ANOVA with Tukey's *post hoc* test, $n = 4$, *** $P < 0.001$). (K, L) Protein expression of IRAK-1 in HCFs stimulated by DOX (0.1 μ M) for 24 h (unpaired *t*-test, $n = 4$, * $P < 0.05$).

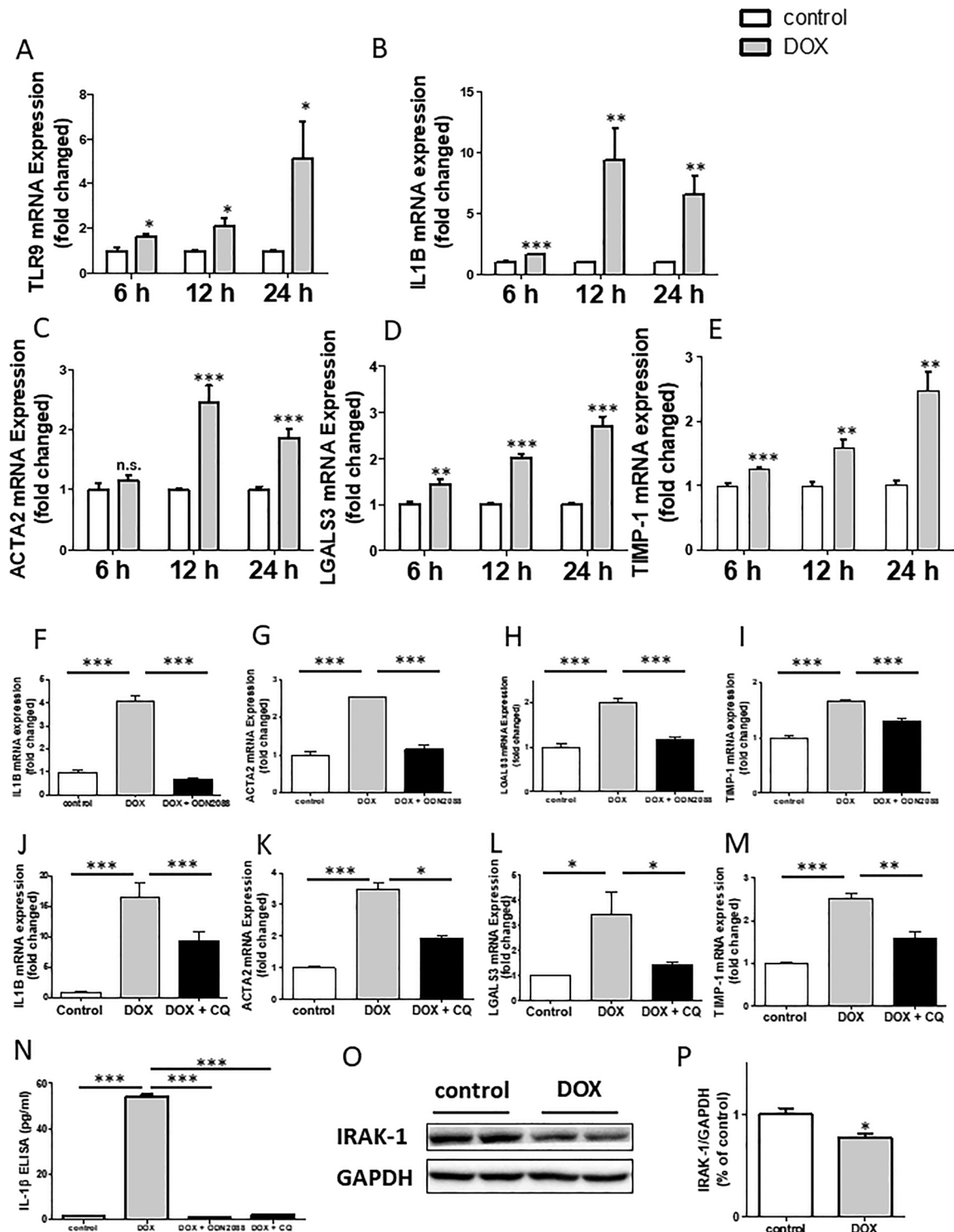


Figure 5 DOX promoted fibrotic response JNK signalling, and pioglitazone attenuated these changes. (A–C) Protein expression of Col1A1, α -SMA, and galectin-3 in HCFs stimulated by DOX (0.1 μ M) for 24 h (unpaired *t*-test, $n = 8-9$, $***P < 0.001$). (D, E) Phosphokinase antibody array was performed in HCFs exposed to DOX for 24 h. DOX activated significantly phosphorylated SAPK/JNK. (F, G) The time course of SAPK/JNK phosphorylation in HCFs stimulated by DOX (0.1 μ M) with or without pioglitazone (10 μ M) for 6, 12, and 24 h (one-way ANOVA with Tukey's *post hoc* test, $n = 4-5$, $**P < 0.01$, $***P < 0.001$). (H–N) Protein expression of Col1A1, α -SMA, and galectin-3 in DOX exposure HCFs (0.1 μ M) with or without pioglitazone (10 μ M) for 24 h (unpaired *t*-test, $n = 4-7$, $**P < 0.01$, $***P < 0.001$). (K, O) The activity of MMP2 and MMP9 by gelatin zymography in DOX exposure HCFs (0.1 μ M) with or without pioglitazone (10 μ M) for 24 h (one-way ANOVA with Tukey's *post hoc* test, $n = 4$, $**P < 0.01$, $***P < 0.001$). (P–R) Immunofluorescence microscopy analysis of α -SMA and galectin-3 expression in DOX-exposed HCFs (0.1 μ M) with or without pioglitazone (10 μ M) for 24 h. Red fluorescence is α -SMA, and green fluorescence is galectin-3; magnification = $\times 40$. The staining intensity of multiple fields was quantified with ImageJ (one-way ANOVA with Tukey's *post hoc* test, $n = 3$, $P < 0.05$).

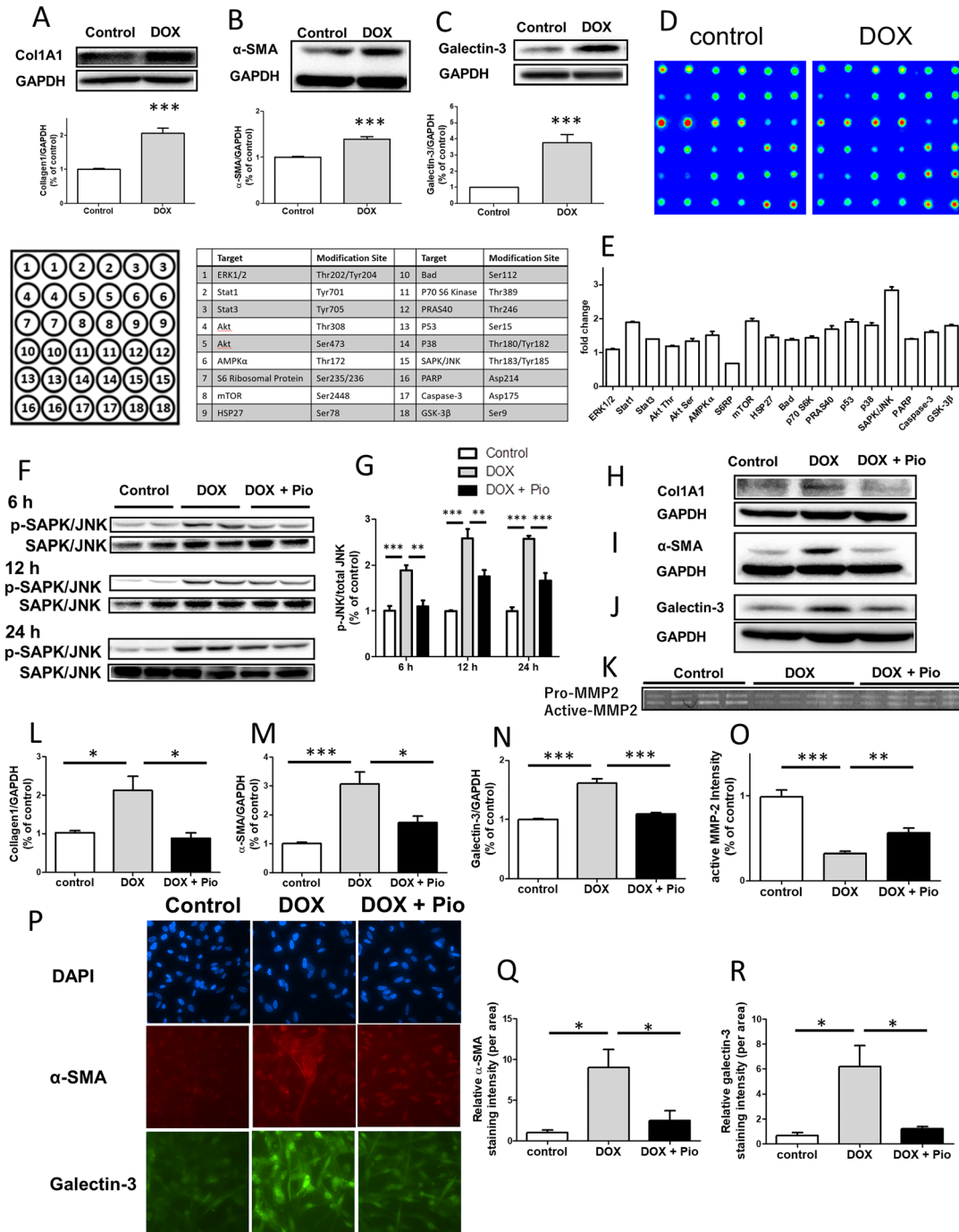


Figure 6 Pioglitazone attenuated low-dose DOX-induced reactive fibrosis in mice. (A) Protocol in experiments to assess the DOX-induced cardiotoxicity in mice. The total cumulative dose of DOX was set to 12 mg/kg. Saline (control) or DOX (4 mg/kg/week for 3 weeks) was administered intraperitoneally. Pioglitazone was administered orally (10 mg/kg/day for 4 weeks). (B, E) Sirius red staining in the perivascular area of heart sections in each group; magnification = $\times 40$. Perivascular fibrotic area in three random fields was measured by ImageJ software (one-way ANOVA with Tukey's *post hoc* test, $n = 4$, $^*P < 0.05$). (C, F) Immunohistochemical staining of α -SMA in the perivascular area of heart sections in each group; magnification = $\times 40$. Arrows show the α -SMA-positive cells. The number of α -SMA-positive cells in the perivascular fibrotic area was counted in three random fields (one-way ANOVA with Tukey's *post hoc* test, $n = 4$, $^{***}P < 0.001$). (D, G) Immunohistochemical staining of galectin-3 in the perivascular area of heart sections in each group; magnification = $\times 40$. Galectin-3-positive area in three random fields was measured by ImageJ software (one-way ANOVA with Tukey's *post hoc* test, $n = 4$, $^{***}P < 0.001$).

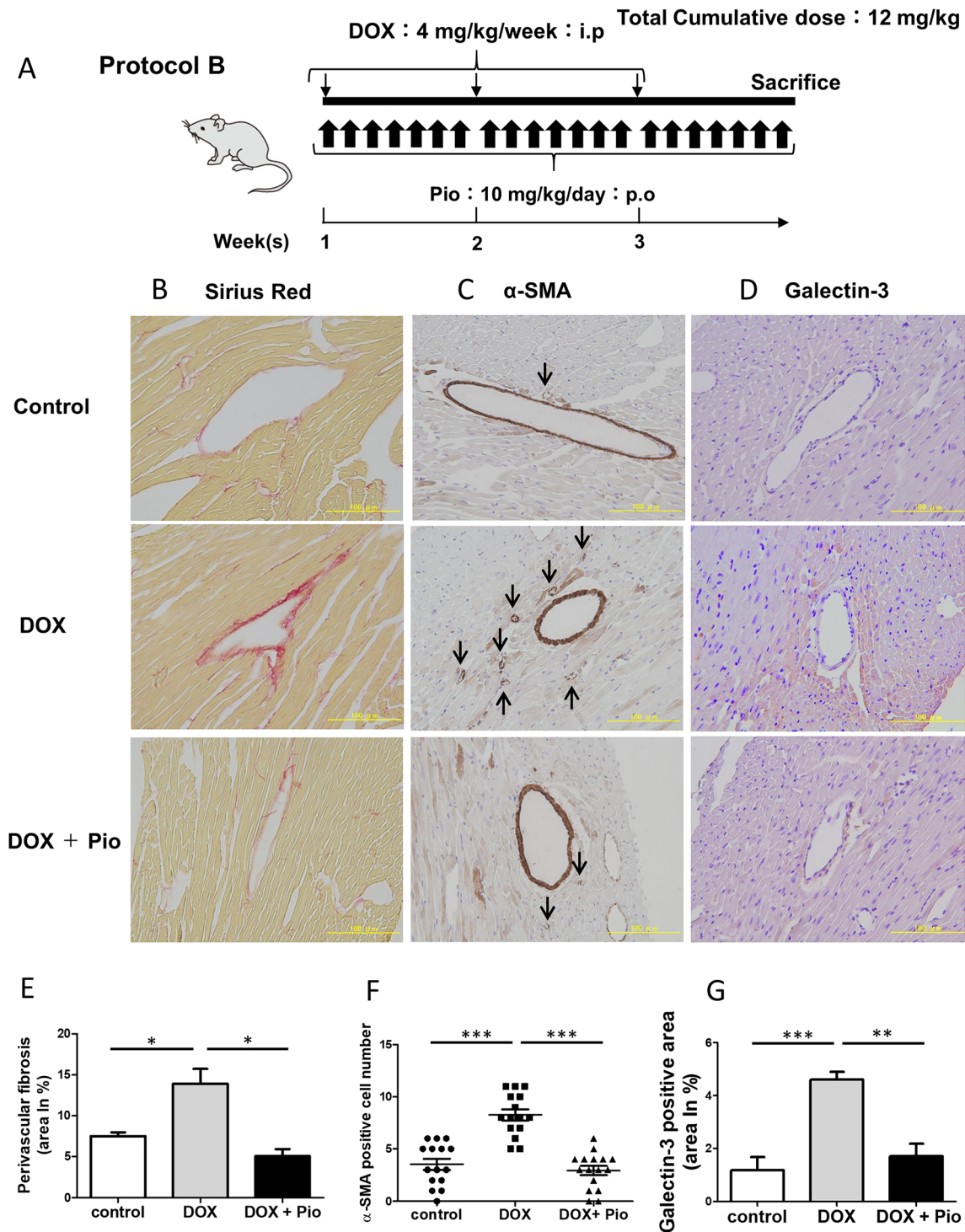
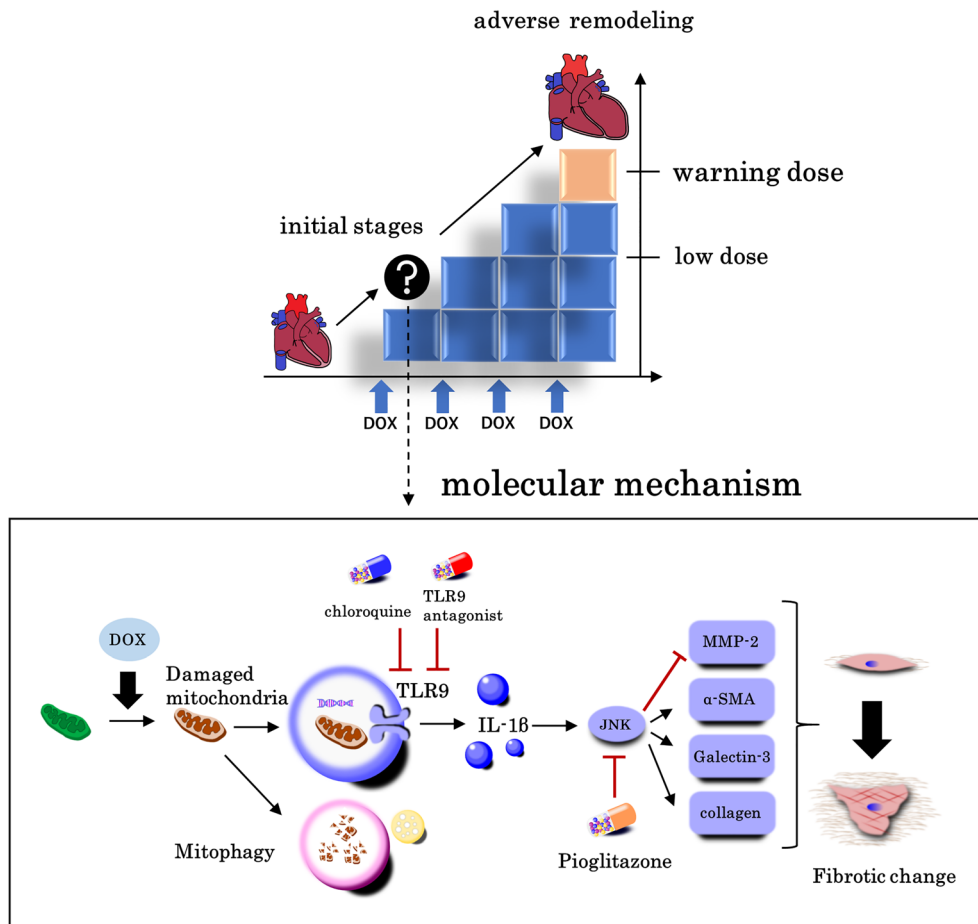


Figure 7 Proposed mechanism of DOX-induced cardiotoxicity on CFs. Reactive fibrosis precedes doxorubicin-induced cardiotoxicity through sterile inflammation by DAMPs released from mitochondria in early stage.



the data. Chemiluminescence detection was performed using the Pierce ECL reagent (Thermo Fisher). Signal intensities of the bands were quantified using ATTO CS Analyzer 4 software (ATTO, Tokyo, Japan).

Cytokine ELISA

The secretion of IL-1 β in the cell culture medium was measured using a human IL-1 β quantitative ELISA kit (R&D Systems Inc., MN, USA) according to the manufacturer's instructions. HCFs were cultured for 24 h, and conditioned media were collected. Samples for IL-1 analysis were not diluted.

Immunofluorescence staining

Immunofluorescence staining was performed as previously described.¹² Cells were then visualized using fluorescence microscopy with an inverted microscope (Nikon, Tokyo,

Japan). Staining intensity was quantified using Image-J software (NIH).

Phosphokinase antibody array

Membrane array experiments were carried out using the PathScan Signaling Antibody Array Kit (Cell Signaling) according to the manufacturer's instructions. Signal intensities were quantified using ATTO CS Analyzer 4 software (ATTO, Tokyo, Japan).

Gelatin zymography

The supernatant from cells cultured with or without DOX for 24 h was collected, and matrix metalloproteinase (MMP) activity was examined by gelatin zymography as described previously.¹⁶ The signal intensities of the bands were quantified using ATTO CS Analyzer 4 software (ATTO, Tokyo, Japan).

Data analysis and statistics

Statistical analysis was performed using GraphPad Prism 5 software (GraphPad Software Inc., CA, USA). Statistical comparisons between groups were performed using Student's *t* test or one-factor analysis of variance with the Tukey's *post hoc* test. The criterion of statistical significance was set at $P < 0.05$.

Results

Low-dose doxorubicin provoked perivascular fibrosis but not cardiomyocyte death in mice

Cardiotoxicity of DOX is cumulative, and the onset of heart failure significantly increases when the total dose is more than 550 mg/m² in humans.¹⁷ We evaluated the effects of DOX at the stage when the cumulative dose had not reached the toxic dose *in vivo* (Figure 1A). The total dose of DOX was set to 12 mg/kg, which corresponded to approximately 400 mg/m² in standard physique humans. Low-dose DOX did not induce significant apoptosis in cardiac tissue of mice (Figure 1B and 1D). Low-dose DOX-induced fibrosis was localized to the perivascular area in mice (Figure 1C and 1E), while the changes in the interstitial area were slight. This result indicated that DOX might induce reactive fibrosis prior to cell apoptosis at the low accumulation stage.

Microarray analysis suggested that low concentrations of doxorubicin activated the innate immune system and induced cardiac remodelling biomarkers

To evaluate the threshold of DOX cytotoxicity in HCFs, we first performed Calcein-A13, Line M, and propidium iodide assays. We found that 0.1 and 0.25 μ M did not significantly affect cell viability or cell apoptosis for 24 h (Figure 2A–2C). In addition, we performed XTT assays. DOX at a concentration of 0.1 μ M did not significantly affect cell proliferation for 24 h (Figure 2D). This concentration was much lower than the previous reports about DOX-induced cardiotoxicity. We used 0.1 μ M DOX, which did not directly induce cell death in this study.

We performed a microarray analysis to evaluate the effect of low-dose DOX on gene expression in HCFs. Genes that increased more than 1.5-fold or decreased less than 0.67-fold in DOX-exposed HCFs were regarded as significantly changed genes; 1526 genes were significantly increased, and 1031 genes were decreased at 6 h; 4104 genes were significantly increased, and 2603 genes were decreased at 24 h (Figure 2E). Enrichment analysis was performed with KEGG pathway

analysis and GSEA. We first focused on some terms among the top 10 in KEGG pathway analysis (Figure 2F). The terms were 'Cytokine-cytokine receptor interaction', 'Rheumatoid arthritis', 'Malaria', and 'Lysosome'. We next assessed the results of GSEA analysis (Figure 2G). Among the significantly changed gene sets, we confirmed a similar tendency in KEGG pathway analysis in GSEA. The gene sets were 'POSITIVE_REGULATION_OF_INFLAMMATORY_RESPONSE', 'CYTOKINE_ACTIVITY', 'RESPONSE_TO_BACTERIUM', 'POSITIVE_REGULATION_OF_RESPONSE_TO_WOUNDING', and 'LYTIC_VACUOLE'. Based on the aforementioned results, we finally examined the individual gene expression changes in inflammatory cytokines involved in the innate immune system and Toll-like receptor (TLR) family. In addition, we evaluated representative cardiac remodelling biomarkers specific for CFs.¹⁸ DOX increased the IL-1 family, IL-12, TLR2, 4, 5, and 9, LGAL3, SPP1, and IL1RL1 after 24 h (Figure 2H and 2I).

Doxorubicin induced mitochondrial damage and mitophagy

We first evaluated mitochondrial activity with MitoTracker Red, depending on the mitochondrial membrane potential of living cells. DOX significantly decreased the mitochondrial membrane potential in HCFs from 6 to 24 h (Figure 3A–3C). We next evaluated mitophagy, which is mitochondrial selective autophagy and processes damaged mitochondria.¹⁹ Mitophagy was significantly induced 6 h after DOX exposure and sustained to 24 h (Figure 3D–3F). The mtDNA copy number and mitochondrial transcription factor A (TFAM) (GenBank accession no. NM003201) were increased. These results were considered a compensatory response to maintain mitochondrial mass (Figure 3G and 3H). In addition, the fluctuations of PI3 Kinase Class III (PI3KC3), p62, and LC3B-II, which were autophagy-related markers, were also consistent with these results (Figure 3I–3L).

Doxorubicin sustainably increased mRNA transcript levels of Toll-like receptor 9, interleukin-1, and profibrotic markers, and chloroquine attenuated these effects in human cardiac fibroblasts

We evaluated the mRNA expression of TLR9 (GenBank accession no. NC000003) and IL1B (GenBank accession no. NM000576), and both significantly increased in DOX-treated HCFs (Figure 4A and 4B). This result indicated that DOX promoted the production of inflammatory cytokines through the damaged mitochondria as an endogenous antigen. IL-1 β is an inflammatory cytokine that promotes adverse cardiac remodelling.²⁰ DOX actually increased the mRNA expression

of LGAL3, ACTA2, and TIMP-1, which were representative cardiac fibrosis markers (GenBank accession no. NM002306, NM001613, and NM003254) (Figure 4C–4E). We next inhibited TLR9, which was located upstream of the CF markers, and evaluated the DOX-induced response in HCFs. ODN2088 (TLR9 antagonist) attenuated the mRNA transcription of IL1B, LGAL3, ACTA2, and TIMP-1 induced by DOX (Figure 4F–4I). TLR9-ligand mediated intracellular signal transduction via ubiquitination of IRAK-1.^{21,22} Chloroquine is frequently used as an inhibitor of TLR9.^{23–27} Chloroquine also attenuated the mRNA transcription of IL1B, LGAL3, ACTA2, and TIMP-1 induced by DOX (Figure 4J–4M). The secretion of IL-1 β was significantly increased 24 h after the DOX treatment. Furthermore, both ODN 2088 and chloroquine inhibited the DOX-induced IL-1 β secretion (Figure 4N). IRAK-1 was degraded in the DOX-treated HCFs (Figure 4K and 4L). These results indicated that the sterile inflammation derived from the damaged mitochondria promoted the fibrotic changes through TLR9 activation.

Doxorubicin promoted the fibrotic response through stress-activated protein kinase/c-Jun NH2-terminal kinase signalling, and pioglitazone attenuated these changes

We evaluated the expression of fibrosis-related biomarkers at the protein level. The protein expression of COL1A1, α -SMA, and galectin-3 was significantly increased 24 h after the DOX treatment (Figure 5A–5C). We screened the phosphorylated proteins using a phosphokinase antibody array. DOX significantly activated phosphorylated SAPK/JNK (Figure 5D and 5E). Then, we assessed the phosphorylation of SAPK/JNK 6, 12, and 24 h after stimulation. DOX remarkably phosphorylated SAPK/JNK (Figure 5F and 5G). We next used pioglitazone, which is a peroxisome proliferator-activated receptor (PPAR γ) agonist, because activated PPAR γ was shown to antagonize SAPK/JNK signalling.²⁸ Pioglitazone attenuated the phosphorylation of SAPK/JNK (Figure 5F and 5G) and suppressed the DOX-induced expression of COL1A1, α -SMA, and galectin-3 (Figure 5H–5J, 5L–5N). The same results were confirmed by immunofluorescence staining (Figure 5P–5R). MMP plays an important role in cardiac remodelling. In particular, MMP-2 and 9 are the main subtypes associated with cardiac fibrosis. Gelatin zymography showed that DOX suppressed the active MMP-2, and pioglitazone recovered this change (Figure 5K and 5O). In addition, we used SP600125 (JNK inhibitor) and GW1929 (non-thiazolidinedione PPAR γ agonist). Both, similarly to pioglitazone, suppressed the DOX-induced expression of α -SMA and galectin-3 (Supporting Information, Figure S1).

Pioglitazone attenuated the doxorubicin-induced fibrotic response in mice

We evaluated the effects of pioglitazone in animal studies. Pioglitazone was orally administered at 10 mg/kg daily (Figure 6A). Pioglitazone attenuated the DOX-induced fibrotic changes and the expression of α -SMA-positive cells and the expression of galectin-3 in the perivascular area (Figure 6B–6G).

Discussion

In the current study, we demonstrated that low-dose DOX, which did not lead to cell death, provoked fibrotic changes. Our results indicated that DOX directly activated CFs and induced the reactive fibrotic response at the initial stage. Furthermore, we demonstrated that the damaged mitochondria functioned as DAMPs and promoted the innate immune system. As a result, DOX provoked fibrotic changes through SAPK/JNK.

We have previously proven that CFs play an important role in various pathologies of heart disease and could be therapeutic targets.²⁹ We hypothesize that CFs contributed to the onset of DOX-induced heart failure and focused on the role of CFs. We first confirmed that low-dose DOX provoked perivascular fibrosis but not cardiomyocyte death in an animal study. The perivascular area is known to be involved in the early stage of reactive fibrosis.³⁰ The total dose was set to 12 mg/kg, which was below the dose for the increased cardiotoxicity. This result indicated that reactive fibrosis preceded the cardiotoxicity of DOX at the initial stage. We performed a microarray analysis and extracted the terms with high commonality from significantly increased gene sets of KEGG pathway analysis and GSEA. Interestingly, we found that several terms and gene sets, which were significantly changed by DOX, had common points. We hypothesized that DOX activated the innate immune system and induced the production of inflammatory cytokines from these terms. Furthermore, several genes known to correlate with adverse cardiac remodelling were increased in DOX-exposed HCFs. Therefore, we also expected that the inflammatory response, which is associated with the innate immune system, promoted adverse cardiac remodelling. Of course, the DOX-induced inflammatory response is non-infectious. The endogenous substances that induce sterile inflammation are called DAMPs.³¹ Damaged mitochondria are well known as DAMPs that activate the innate immune system.³² DAMPs derived from mitochondria include the damaged mitochondria itself, mtDNA, TFAM, and so on.³³ These molecules are recognized by pattern recognition receptors. There are five classes known to pattern recognition receptors. The TLR family is the best known molecule.³⁴ TLRs recognize DAMPs and

induce an inflammatory response mainly through the production of IL-1.³⁵ DAMPs released from mitochondria mainly bind to TLR9, produce IL-1 β , and induce the inflammatory response.^{33,36} Moreover, in cardiomyocytes, DAMPs activated TLR9 treated with DOX.³⁷ DOX decreased mitochondrial membrane potential in an early stage. At the same time, DOX induced the mitophagy that degrades damaged mitochondria. In addition, mtDNA copy number and TFAM were increased. These results were considered a compensatory response to maintain mitochondrial mass. This compensatory response was also reported in a sepsis model.³⁸ Furthermore, the mRNA expression of TLR9, which specifically recognizes mitochondrial-derived DAMPs, was increased. The mRNA of IL1B and the secretion of IL-1 β were continuously increased. These responses were attenuated by TLR9 antagonist. Furthermore, chloroquine, which inhibited lysosomal action and TLR9 activity, also attenuated the production of IL-1 β . TLR9-ligand mediated intracellular signal transduction via ubiquitination of IL-1R-associated kinase 1 (IRAK1). IRAK1 was degraded in the DOX-treated HCFs. This finding was consistent with our hypothesis that the damaged mitochondria by DOX activated the innate immune system via TLR9 to induce an inflammatory response. In general, mitophagy degrades damaged mitochondria and works defensively. However, our results indicated that DOX did not suppress inflammatory cytokines. This result might be caused by insufficient degradation of the mitochondrial substrate.³⁹ In addition, it is possible that the degradation of mitochondrial substrate does not catch up with the occurrence of damaged mitochondria. There is no doubt that the damaged mitochondria and their compensatory response are important for DOX-induced pathology.

We confirmed that DOX enhanced the expression of biomarkers of adverse cardiac remodelling. CFs differentiate into myofibroblasts and promote the production of ECM and inflammatory cytokines when activated. Myofibroblasts express α -SMA, which is a specific cell marker.⁸ Galectin-3 is increased in patients with heart failure and is highly correlated with cardiac fibrosis as a biomarker.⁴⁰ TIMP-1 is a molecule that inhibits the activity of MMPs.³² TIMP-1 inhibits the degradation of ECM and delays ECM turnover. It leads to the accumulation of collagen. We confirmed that TLR9 antagonist and chloroquine attenuated the mRNA expression of these markers. Furthermore, inflammatory cytokines are known to promote cardiac fibrosis and adverse cardiac remodelling. We confirmed that chloroquine attenuated the mRNA expression of IL1B. As shown previously, we demonstrated that the sterile inflammation derived from the damaged mitochondria, which was evoked by low-dose DOX, promotes adverse cardiac remodelling. We thought that the suppression of this pathway might be able to treat DOX-induced cardiotoxicity. Chloroquine has serious side effects such as retinopathy⁴¹ and itself has cardiotoxicity.^{42–44} Moreover, it is very expensive. Therefore, it is difficult to use chloroquine

for prophylaxis for cardiotoxicity. We then focused on the SAPK/JNK pathway activated by DOX-treated HCFs because the phosphokinase antibody array showed that DOX significantly activated phosphorylated SAPK/JNK.²⁸ However, SAPK/JNK inhibitor is not available in clinical. One of the purposes in the current study was to make a practical and useful clinical proposal. Therefore, we examined whether pioglitazone exerts its suppressive effects on SAPK/JNK because PPAR γ antagonize SAPK/JNK signalling. Pioglitazone is a ligand to PPAR γ and is mainly used for diabetes. Pioglitazone suppresses large adipocytes, which secrete inflammatory cytokines and improve insulin resistance. Pioglitazone suppressed the protein expression of α -SMA, galectin-3, and collagen and recovered the active MMP-2 through the suppression of SAPK/JNK signalling. Further, we performed an additional study using SAPK/JNK inhibitor and non-thiazolidinedione PPAR γ agonist. Both, similarly to pioglitazone, suppressed the DOX-induced fibrotic response via attenuating phosphorylated SAPK/JNK signalling. These results suggest that pioglitazone inhibits SAPK/JNK and exhibits cardioprotective effects. Moreover, pioglitazone also suppressed DOX-induced perivascular fibrosis in animal studies. As a limitation, pioglitazone mainly acts on adipocytes to show some physiological actions; therefore, it might be difficult to evaluate the direct effect of pioglitazone on CFs *in vivo*. In addition, we evaluated perivascular fibrosis *in vivo* study. In the pathological features that consensus on DOX cardiomyopathy, it indicates myofibrillar disarray, shedding, vacuoles, and myocardial necrosis⁴⁵. They have not reported about perivascular fibrosis. However, these are features just after heart failure has already occurred. There are very few reports about human myocardial biopsy, which were performed in the early stages before the onset of heart failure. Therefore, it requires further extensive work to elucidate the mechanism of DOX-induced cardiotoxicity at early stage in the future.

So far, many reports have focused on the pathophysiology after the onset of severe myocardial injury by DOX. In this study, we focused on the phenomenon that occurred in the early stage before the progression of the cardiotoxicity. Perivascular fibrosis is specific as an initial change of reactive fibrosis. It is well known that pathological changes spread from perivascular fibrosis and lead to heart failure with preserved ejection fraction, such as hypertensive cardiomyopathy⁴⁶ and diabetic cardiomyopathy.⁴⁷ Therefore, it is reasonable to assume that DOX-induced perivascular fibrosis without cell death in the initial stage develops into extensive fibrosis and myocardial dysfunction. This also explains that the cardiotoxicity of DOX is cumulative and manifests when DOX exceeds a certain amount after repeated administration. However, there are some limitations in the present study. We did not directly show that perivascular fibrosis was transferred to myocardial injury. More detailed analysis will be necessary to examine the mechanism of cardiotoxicity. The

accumulation of long-term follow-up data will be required in future animal studies. We need to observe the pathological changes at various points and check the overall progression of fibrosis. Similarly, further study will be required to investigate whether pioglitazone can prevent perivascular fibrosis from the development of cardiotoxicity.

The novelty of this paper is as follows. (i) We investigated initial cardiac remodelling before reaching the toxic dose with low-dose DOX in CFs. (ii) We demonstrated that the low dose of DOX directly induced 'reactive fibrosis', not 'replacement fibrosis', in CFs. (iii) We proved that the low dose of DOX induced the fibrotic response through the sterile inflammation induced by damaged mitochondria. (iv) We showed that PPAR γ agonists had the potential to attenuate DOX-induced cardiotoxicity. We propose the potential mechanism of progression of DOX-induced heart failure, as shown in *Figure 7*. We believe that these discoveries identify a new mechanism and contribute to the prophylaxis and treatment of DOX-induced heart failure.

Acknowledgements

The authors are grateful to Akane Nagasako and Yoko Ike.

Funding

This study was supported in part by the Japan Society for the Promotion of Science (JSPS) KAKENHI grant (24390200, 25670131 to Y.I.; 26870481 to M.U.); the Ministry of Education, Culture, Sports, Science and Technology (MEXT) KAKENHI grant (22136009 to Y.I.); and the Japan Agency for Medical Research and Development (AMED; 66890005, 66890011, 66890001, 66890023 to Y.I.).

References

1. Armstrong GT, Kawashima T, Leisenring W, Stratton K, Stovall M, Hudson MM, Sklar CA, Robison LL, Oeffinger KC. Aging and risk of severe, disabling, life-threatening, and fatal events in the childhood cancer survivor study. *J Clin Oncol* 2004; **32**: 1218–1227.
2. Suter TM, Procter M, Van Veldhuisen DJ, Muscholl M, Bergh J, Carlomagno C, Perren T, Passalacqua R, Bighin C, Klijn JG, Ageev FT. Trastuzumab-associated cardiac adverse effects in the herceptin adjuvant trial. *J Clin Oncol* 2007; **25**: 3859–3865.
3. Oeffinger KC, Mertens AC, Sklar CA, Kawashima T, Hudson MM, Meadows AT, Friedman DL, Marina N, Hobbie W, Kadan-Lottick NS, Schwartz CL, Leisenring W, Robison LL. Childhood Cancer Survivor Study. Chronic health conditions in adult survivors of childhood cancer. *N Engl J Med* 2006; **355**: 1572–1582.
4. Link G, Tirosh R, Pinson A, Hershko C. Role of iron in the potentiation of anthracycline cardiotoxicity: identification of heart cell mitochondria as a major site of iron-anthracycline interaction. *J Lab Clin Med* 1996; **127**: 272–278.
5. Hanna AD, Lam A, Tham S, Dulhunty AF, Beard NA. Adverse effects of doxorubicin and its metabolic product on cardiac RyR2 and SERCA2A. *Mol Pharmacol* 2014; **86**: 438–449.
6. Zhang S, Liu X, Bawa-Khalife T, Lu LS, Lyu YL, Liu LF, Yeh ET. Identification of the molecular basis of doxorubicin-induced cardiotoxicity. *Nat Med* 2012; **18**: 1639–1642.
7. Banerjee I, Fuseler JW, Price RL, Borg TK, Baudino TA. Determination of cell types and numbers during cardiac development in the neonatal and adult rat and mouse. *Am J Physiol Heart Circ Physiol* 2007; **293**: H1883–H1891.
8. Talman V, Ruskoaho H. Cardiac fibrosis in myocardial infarction—from repair and remodeling to regeneration. *Cell Tissue Res* 2016; **365**: 563–581.
9. Russo I, Frangiannis NG. Diabetes-associated cardiac fibrosis: cellular

Conflicts of interest

None declared.

Supporting information

Additional supporting information may be found online in the Supporting Information section at the end of the article.

Table S1. The sequences of the specific primers in this study.

Figure S1. DOX promoted the fibrotic response through SAPK/JNK signalling. SAPK/JNK inhibitor and non-thiazolidinedione PPAR γ agonist attenuated these changes like pioglitazone.

Figure S2. Representative western blots of the p-PI3KC3, PI3KC3, p62 and LC3BII in HCFs treated by DOX.

Figure S3. Representative western blots of the IRAK-1 in HCFs treated by DOX.

Figure S4. Representative western blots of the COL1A1, α -SMA, and Galectin-3 in HCFs treated by DOX.

Figure S5. Representative western blots of the phosphorylated SAPK/JNK and SAPK/JNK treated by DOX with or without pioglitazone.

Figure S6. Representative western blots of the COL1A1, α -SMA, and Galectin-3 treated by DOX with or without pioglitazone.

Figure S7. Representative western blots of the phosphorylated SAPK/JNK, SAPK/JNK, α -SMA and Galectin-3 treated by DOX with or without SP600125 or GW1929.

- effectors, molecular mechanisms and therapeutic opportunities. *J Mol Cell Cardiol* 2016; **90**: 84–93.
10. van der Pal HJ, van Dalen EC, van Delden E, van Dijk IW, Kok WE, Geskus RB, Sieswerda E, Oldenburger F, Koning CC, van Leeuwen FE, Caron HN, Kremer LC. High risk of symptomatic cardiac events in childhood cancer survivors. *J Clin Oncol* 2012; **30**: 1429–1437.
 11. Zamorano JL, Lancellotti P, Rodriguez Muñoz D, Aboyans V, Asteggiano R, Galderisi M, Habib G, Lenihan DJ, Lip GYH, Lyon AR, Lopez Fernandez T, Mohty D, Piepoli MF, Tamargo J, Torbicki A, Suter TM. 2016 ESC Position paper on cancer treatments and cardiovascular toxicity developed under the auspices of the ESC committee for practice guidelines: The Task force for cancer treatments and cardiovascular toxicity of the European Society of Cardiology (ESC). *Eur Heart J* 2016; **37**: 2768–2801.
 12. Tanaka R, Umemura M, Narikawa M, Fujita T, Yokoyama U, Ishigami T, Kimura K, Tamura K, Ishikawa Y. Hydrostatic pressure suppresses fibrotic changes via Akt/GSK-3 signaling in human cardiac fibroblasts. *Physiol Rep* 2018; **6**: e13687.
 13. Akimoto T, Umemura M, Nagasako A, Ohtake M, Fujita T, Yokoyama U, Eguchi H, Yamamoto T, Ishikawa Y. Alternating magnetic field enhances cytotoxicity of compound C. *Cancer Sci* 2018; **109**: 3483–3493.
 14. Nakakaji R, Umemura M, Mitsudo K, Kim JH, Hoshino Y, Sato I, Masuda T, Yamamoto M, Kioi M, Koizumi T, Fujita T, Yokoyama U, Iida M, Sato M, Sato H, Murofushi S, Shibata S, Aoki I, Eguchi H, Tohnai I, Ishikawa Y. Treatment of oral cancer using magnetized paclitaxel. *Oncotarget* 2018; **9**: 15591–15605.
 15. Umemura M, Baljinnam E, Feske S, De Lorenzo MS, Xie LH, Feng X, Oda K, Makino A, Fujita T, Yokoyama U, Iwatsubo M, Chen S, Goydos JS, Ishikawa Y, Iwatsubo K. Store-operated Ca²⁺ entry (SOCE) regulates melanoma proliferation and cell migration. *PLoS ONE* 2014; **9**: e89292.
 16. Yokoyama U, Ishiwata R, Jin MH, Kato Y, Suzuki O, Jin H, Ichikawa Y, Kumagaya S, Katayama Y, Fujita T, Okumura S, Sato M, Sugimoto Y, Aoki H, Suzuki S, Masuda M, Minamisawa S, Ishikawa Y. Inhibition of EP4 signaling attenuates aortic aneurysm formation. *PLoS ONE* 2012; **7**: e36724.
 17. Von Hoff DD, Layard MW, Basa P, Davis HL Jr, Von Hoff AL, Rozenzweig M, Muggia FM. Risk factors for doxorubicin-induced congestive heart failure. *Ann Intern Med* 1979; **91**: 710–717.
 18. Holzhauser L, Kim G, Sayer G, Uriel N. The effect of left ventricular assist device therapy on cardiac biomarkers: implications for the identification of myocardial recovery. *Curr Heart Fail Rep* 2018; **15**: 250–259.
 19. Okamoto K, Kondo N. Mitochondria and autophagy: critical interplay between the two homeostats. *Biochim Biophys Acta* 2012; **1820**: 595–600.
 20. Bujak M, Dobaczewski K, Chatila K, Mendoza LH, Li N, Reddy A, Frangogiannis NG. Interleukin-1 receptor type I signaling critically regulates infarct healing and cardiac remodeling. *Am J Pathol* 2008; **173**: 57–67.
 21. Kong F, Liu Z, Jain VG, Shima K, Suzuki T, Muglia LJ, Starczynowski DT, Pasare C, Bhattacharyya S. Inhibition of IRAK1 ubiquitination determines glucocorticoid sensitivity for TLR9-induced inflammation in macrophages. *J Immunol* 2017; **199**: 3654–3667.
 22. Uematsu S, Sato S, Yamamoto M, Hirotsani T, Kato H, Takeshita F, Matsuda M, Coban C, Ishii KJ, Kawai T, Takeuchi O, Akira S. Interleukin-1 receptor-associated kinase-1 plays an essential role for Toll-like receptor (TLR)7- and TLR9-mediated interferon-alpha induction. *J Exp Med* 2005; **201**: 915–923.
 23. Ye W, Tang X, Yang Z, Liu C, Zhang X, Jin J, Lyu J. Plasma-derived exosomes contribute to inflammation via the TLR9-NF-κB pathway in chronic heart failure patients. *Mol Immunol* 2017; **87**: 114–121.
 24. Torigoe M, Sakata K, Ishii A, Iwata S, Nakayamada S, Tanaka Y. Hydroxychloroquine efficiently suppresses inflammatory responses of human class-switched memory B cells via Toll-like receptor 9 inhibition. *Clin Immunol* 2018; **195**: 1–7.
 25. Zhang Y, Li Y, Li R, Ma Y, Wang H, Wang Y. Chloroquine inhibits MGC803 gastric cancer cell migration via the Toll-like receptor 9/nuclear factor kappa B signaling pathway. *Mol Med Rep* 2015; **11**: 1366–1371.
 26. Liu M, Peng J, Tai N, Pearson JA, Hu C, Guo J, Hou L, Zhao H, Wong FS, Wen L. Toll-like receptor 9 negatively regulates pancreatic islet beta cell growth and function in a mouse model of type 1 diabetes. *Diabetologia* 2018; **61**: 2333–2343.
 27. Yasuda H, Leelahavanichkul A, Tsunoda S, Dear JW, Takahashi Y, Ito S, Hu X, Zhou H, Doi K, Childs R, Klinman DM, Yuen PS, Star RA. Chloroquine and inhibition of Toll-like receptor 9 protect from sepsis-induced acute kidney injury. *Am J Physiol Renal Physiol* 2008; **294**: 1050–1058.
 28. Hsu WH, Lee BH, Liao TH, Hsu YW, Pan TM. Monascus-fermented metabolite monascin suppresses inflammation via PPAR-γ regulation and JNK inactivation in THP-1 monocytes. *Food Chem Toxicol* 2012; **50**: 1178–1186.
 29. Narikawa M, Umemura M, Tanaka R, Fujita T, Yokoyama U, Ishigami T, Kimura K, Tamura K, Ishikawa Y. Acute hyperthermia inhibits TGF-β1-induced cardiac fibroblast activation via suppression of Akt signaling. *Sci Rep* 2018; **8**: 6277.
 30. Kai H, Mori T, Tokuda K, Takayama N, Tahara N, Takemiya K, Kudo H, Sugi Y, Fukui D, Yasukawa H, Kuwahara F, Imaizumi T. Pressure overload-induced transient oxidative stress mediates perivascular inflammation and cardiac fibrosis through angiotensin II. *Hypertens Res* 2006; **29**: 711–718.
 31. Schaefer L. Complexity of danger: the diverse nature of damage-associated molecular patterns. *J Biol Chem* 2014; **289**: 35237–35245.
 32. Krysko DV, Agostinis P, Krysko O, Garg AD, Bachert C, Lambrecht BN, Vandenabeele P. Emerging role of damage-associated molecular patterns derived from mitochondria in inflammation. *Trends Immunol* 2016; **32**: 157–164.
 33. Zhang Q, Raouf M, Chen Y, Sumi Y, Sursal T, Junger W, Brohi K, Itagaki K, Hauser CJ. Circulating mitochondrial DAMPs cause inflammatory responses to injury. *Nature* 2010; **464**: 104–107.
 34. Bao W, Xia H, Liang Y, Ye Y, Lu Y, Xu X, Duan A, He J, Chen Z, Wu Y, Wang X, Zheng C, Liu Z, Shi S. Toll-like receptor 9 can be activated by endogenous mitochondrial DNA to induce podocyte apoptosis. *Sci Rep* 2016; **6**: 22579.
 35. Martin SJ. Cell death and inflammation: the case for IL-1 family cytokines as the canonical DAMPs of the immune system. *FEBS J* 2016; **283**: 2599–2615.
 36. Gu X, Wu G, Yao Y, Zeng J, Shi D, Lv T, Luo L, Song Y. Intratracheal administration of mitochondrial DNA directly provokes lung inflammation through the TLR9-p38 MAPK pathway. *Free Radic Biol Med* 2015; **83**: 149–158.
 37. Li M, Sala V, De Santis MC, Cimino J, Cappello P, Pianca N, Di Bona A, Margaria JP, Martini M, Lazzarini E, Pirozzi F, Rossi L, Franco I, Bornbaum J, Heger J, Rohrbach S, Perino A, Tocchetti CG, Lima BHF, Teixeira MM, Porporato PE, Schulz R, Angelini A, Sandri M, Ameri P, Sciarretta S, Lima-Júnior RCP, Mongillo M, Zaglia T, Morello F, Novelli F, Hirsch E, Ghigo A. Phosphoinositide 3-kinase gamma inhibition protects from anthracycline cardiotoxicity and reduces tumor growth. *Circulation* 2018; **138**: 696–711.
 38. Widdrington JD, Gomez-Duran A, Pyle A, Ruchaud-Sparagano MH, Scott J, Baudouin SV, Rostron AJ, Lovat PE, Chinnery PF, Simpson AJ. Exposure of monocytic cells to lipopolysaccharide induces coordinated endotoxin tolerance, mitochondrial biogenesis, mitophagy, and antioxidant defenses. *Front Immunol* 2018; **9**: 2217.
 39. Oka T, Hikoso S, Yamaguchi O, Taneike M, Takeda T, Tamai T, Oyabu J, Murakawa T, Nakayama H, Nishida K, Akira S, Yamamoto A, Komuro I, Otsu K. Mitochondrial DNA that escapes from autophagy causes inflammation and heart failure. *Nature* 2012; **485**: 251–255.

40. Ho JE, Liu C, Lyass A, Courchesne P, Pencina MJ, Vasan RS, Larson MG, Levy D. Galectin-3, a marker of cardiac fibrosis, predicts incident heart failure in the community. *J Am Coll Cardiol* 2012; **60**: 1249–1256.
41. Duncker G, Schmiederer M, Bredehorn T. Chloroquine-induced lipidosis in the rat retina: a functional and morphological study. *Ophthalmologica* 1995; **209**: 79–83.
42. Tselios K, Gladman DD, Harvey P, Mak S, Chantal M, Butany J, Urowitz MB. Hydroxychloroquine-induced cardiomyopathy in systemic lupus erythematosus. *J Clin Rheumatol* 2016; **22**: 287–288.
43. Yogasundaram H, Hung W, Paterson ID, Sergi C, Oudit GY. Chloroquine-induced cardiomyopathy: a reversible cause of heart failure. *ESC Heart Fail* 2018; **5**: 372–375.
44. Fragasso G, Sanvito F, Baratto F, Martinenghi S, Doglioni C, Margonato A. Cardiotoxicity after low-dose chloroquine antimalarial therapy. *Heart Vessels* 2009; **24**: 385–387.
45. Ewer MS, Lippman SM. Type II Chemotherapy-related cardiac dysfunction: time to recognize a new entity. *J Clin Oncol* 2005; **23**: 2900–2902.
46. Kuwahara F, Kai H, Tokuda K, Kai M, Takeshita A, Egashira K, Imaizumi T. Transforming growth factor- β function blocking prevents myocardial fibrosis and diastolic dysfunction in pressure-overloaded rats. *Circulation* 2002; **106**: 130–135.
47. Widyantoro B, Emoto N, Nakayama K, Anggrahini DW, Adiarto S, Iwasa N, Yagi K, Miyagawa K, Rikitake Y, Suzuki T, Kisanuki YY, Yanagisawa M, Hirata K. Endothelial cell-derived endothelin-1 promotes cardiac fibrosis in diabetic hearts through stimulation of endothelial-to-mesenchymal transition. *Circulation* 2010; **121**: 2407–2418.